Journal of Applied Fluid Mechanics, Vol. 13, No. 2, pp. 413-427, 2020.
Available online at www.jafmonline.net, ISSN 1735-3572, EISSN 1735-3645.
DOI: 10.29252/jafm.13.02.30061

A Comparative CFD Study on Laminar and Turbulent Flow Fields in Dual-Rushton Turbine Stirred Vessels

L. C. Li[1†], N. Chen[2], K. F. Xiang[1] and B. P. Xiang[1]

[1] *Key Laboratory of Testing Technology for Manufacturing Process of Ministry of Education, Southwest University of Science and Technology, Mianyang, Sichuan 621010, China*
[2] *Yinhe Constructional and Chemicals Group Co., Ltd. Anxian, Sichuan 622656, China*

†*Corresponding Author Email: tchllc@126.com*

(Received January 21, 2019; accepted July 5, 2019)

ABSTRACT

A computational fluid dynamics(CFD) simulation was carried out to study on flow field characteristics in dual-Rusthton turbine stirred vessels in laminar and turbulent regimes. Model validation was conducted using experimental data in the literature. The simulation results show that flow pattern and dimensionless velocity distribution vary with Reynolds number in laminar regime, while these parameters remain almost unchanged for different Reynolds numbers in turbulent regime. For vessels with a certain geometrical configuration, flow pattern, dimensionless velocity distribution and impeller power number depend mainly on Reynolds number, and are little affected by working medium and enlargement scale. By changing impeller spacing and off-bottom clearance of lower impeller, it is obtained the parallel, merging and diverging flow patterns in turbulent regime, and the changing processes of flow patterns in laminar regime for the three configurations. Total power number has the order of parallel>diverging>merging for the three configurations at the same Reynolds number. With increasing of Reynolds number, the power number of merging configuration shows the largest drop, followed by diverging configuration, and the lowest drop for parallel configuration in laminar regime, while power number rises slightly for the three configurations in turbulent regime.

Keywords: Stirred vessel; Dual-impeller; Numerical simulation; Laminar and turbulent flow; Flow pattern.

NOMENCLATURE

C_1	lower impeller clearance from the vessel bottom
C_2	impeller spacing
C_3	upper impeller clearance from the liquid surface
$C_{1\varepsilon}$,$C_{2\varepsilon}$	standard κ-ε model constants
CFD	Computational Fluid Dynamics
D	impeller diameter
g	gravitational acceleration
G_b	production of turbulent kinetic energy due to buoyancy
G_κ	production of turbulent kinetic energy due to mean velocity gradients
H	liquid level
κ	kinetic energy
LDA	Laser-Doppler Anemometer
MRF	Multiple Reference Frame
N	impeller speed
Np	impeller power number
p	static pressure
P	power consumption
r	radial location in the vessel
R	vessel radius
Re	Reynolds number
t	fluid flow time
T	vessel internal diameter
T_0	impeller torque
u_i	liquid mean velocity of i component
u_i'	fluctuating velocity of i component
u_r	radial velocity
u_{tip}	velocity at blade tip
Y_M	effect of the fluctuating dilatation in compressible turbulence on the overall dissipation rate
z	axial location in the vessel
δ_{ij}	kronecker delta
ε	turbulent energy dissipation rate
μ	molecular viscosity
μ_t	turbulent viscosity
ρ	density
σ_κ , σ_ε	standard κ-ε turbulent model constants

1. INTRODUCTION

Stirred vessels are high efficient mixing equipments, and widely used in many industrial processes, such as chemical, metallurgy, pharmaceutical and wastewater treatment, etc. In many applications, fluid flow in a stirred vessel is in turbulent regime to improve the mixing efficiency. Fluid flow in laminar regime is often regarded as poor mixing and has limited researches by scholars. However, the operations of stirred vessels in laminar regime are also applied in some industrial processes. For example, for high viscosity fluids mixing, it requires very high impeller speed and power consumption to achieve the fluid flow in turbulent regime. The very high speed may destroy impeller blades, resulting in the unsafety of stirred vessels. Therefore, the mixing of many high viscosity fluids is often operated in laminar flow regime in vessels (Lamberto *et al.*, 1996 and 1999; Ascanio *et al.*, 2002). In addition, for some bioreactors, laminar flow regime is recommended for avoiding shear sensitive cell death and destruction of long chain of macromolecules, etc. (Cherry and Papoutsakis, 1988; Millward *et al.*, 1994; Croughan *et al.*, 2000).

Dual-impeller and multi-impeller systems are often applied in many industries, due to the advantages of less land occupation, longer residence time and lower power consumption per impeller in comparison with single impeller systems. Furtherly, Gogate *et al.* (2000) reviewed in detail about the advantages of dual-impeller and multi-impeller systems. In the literature, many researchers have studied flow field, mixing and power consumption in multi-impeller stirred vessels. Rutherford *et al.* (1996) and Micale *et al.* (1999) found out that fluid flow in vessels stirred by dual Rushton turbines forms three typical flow patterns, i.e., parallel, merging and diverging flow patterns, by changing impeller spacing and off-bottom clearance of lower impeller. Liu *et al.* (2008) studied turbulent characteristics in a dual-Rushton turbine stirred vessel using particle image velocimetry (PIV) technique. They also observed the three basic flow patterns and further measured average velocity, trailing vortices and shear strain rate distribution for the three patterns. In addition, other researchers such as Pan *et al.* (2008), Mao (1998) and Weng (1983) also studied flow fields in multi-impeller stirred vessels. Mixing is the main function for a stirred vessel. Mixing time is usually used to determine mixing characteristics, which means the time required to achieve desired or specified degree of homogeneity. Mahmoudi *et al.* (1992) reported that flow patterns affect mixing time in dual-Rushton turbine vessels. On average, merging flow pattern obtained the smallest mixing time for the three patterns. Miao *et al.* (2006) found that mixing time with multi-impeller is longer than that of single impeller when using Rushton turbines, while that is almost the same for multi-impeller systems of other hydrofoil impellers. Besides, scholars such as Foucault *et al.* (2006), Kasat and Pandit (2004), and Abradi *et al.* (1988) researched mixing characteristics in stirred vessels with different impeller combinations. Power consumption is also an important parameter for stirred vessels. For multi-impeller systems, power consumption depends not only on operating conditions and geometrical parameters, but also impeller combinations. Hudcova *et al.* (1989) observed that total power number increases firstly with increasing of impeller spacing, and then reach to the sum of each impeller power number in a dual-disc turbine stirred vessel. Rutherford *et al.* (1996) found that total power number is largest for parallel flow, followed by diverging flow and the lowest for merging flow pattern in dual-Rushton turbine systems. Moreover, Puthli *et al.* (2005) investigated power consumption of impeller combinations with Rushton turbine and pitch blade turbine. Woziwodzki *et al.* (2010) studied power consumption and transitional mixing in eccentric stirred vessels equipped with different impeller combinations, etc.

Except for experimental researches, computational fluid dynamics (CFD) technique is also widely used to study on the hydraulic characteristics in stirred vessels. Many scholars have CFD studied hydraulic characteristics in stirred vessels, and the reliability and accuracy of the CFD method have been verified by experimental data. Nevertheless, up to now, including the literature of above reviews, more experimental and CFD studies are about hydrodynamics in turbulent flow regime in stirred vessels. The researches on flow field characteristics in laminar regime are limited. Some researchers studied laminar flow field in the vessel stirred by a single impeller (Albert *et al.*, 1995; Bakker *et al.*, 1996; Fan *et al.*, 2004; Rice *et al.*, 2006). For multi-impeller systems, Zalc *et al.* (2001, 2002) experimentally and CFD studied laminar flow field in a vessel stirred by three Rushton turbines with Reynolds number ranged from 20 to 100. They observed that flow fields change with Reynolds numbers in the triple-impeller stirred vessel.

As the researches reviewed above, many scholars (Rutherford *et al.*, 1996; Ranade *et al.*, 1997; Micale *et al.*, 1999; Liu *et al.*, 2008; Li *et al.*, 2007; Pan *et al.*, 2008) found that parallel, diverging and merging flow patterns formed in turbulent regime in dual-Rushton turbine stirred vessels by changing the geometrical configuration. Nevertheless, flow field characteristics in laminar regime for the dual-Rushton turbine system with different geometrical configurations are few reported. Thus, in this work, a comparative CFD study was performed to investigate laminar and turbulent flow field characteristics in a stirred vessel equipped with two Rushton turbines. The model validation was performed firstly, and then, the effects of Reynolds number, working medium, enlarge scale and geometrical configuration on laminar and turbulent flow field characteristics were investigated.

2. NUMERICAL MODELS AND SIMULATION METHODS

2.1 Simulation Domain

Geometries of the stirred vessels were shown in

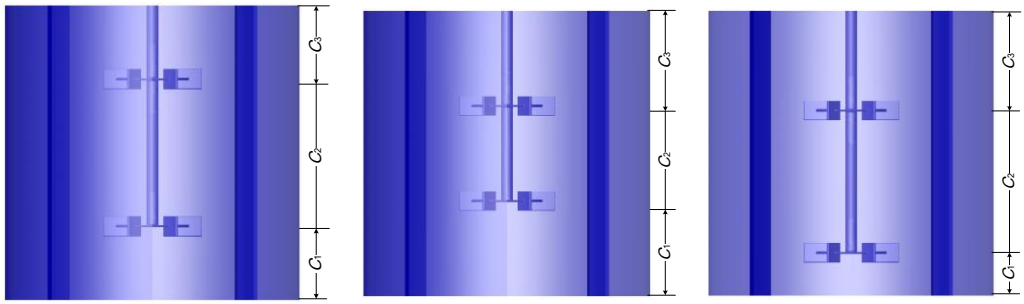

(a) Parallel (b)Merging (c)Diverging

Fig. 1. Geometries of the stirred vessel with different configurations.

Table 1 Parameters for different geometrical configurations

Parameter	Parallel	Merging	Diverging
C_1	0.25T	0.33T	0.15T
C_2	0.5T	0.33T	0.5T
C_3	0.25T	0.33T	0.35T

Table 2 Physical properties of working media in the simulation

Working media	Glycerol concentration	Density (kg m^{-3})	Viscosity (Pa·s)	Refs.
Water	0	998.2	0.001	--
Glycerol + water	75%	1191	0.0262	Woziwodzki *et al.* (2010)
Glycerol + water	94%	1250	0.4	Liang *et al.* (2015)
Glycerol	100%	1260	1.16	Fan *et al.* (2004)

Fig. 1, which were almost the same as the experimental vessels in the literature (Rutherford *et al.*, 1996; Micale *et al.*, 1999). Simulations were carried out in a cylindrical, flat bottom vessel with internal diameter T=0.294 m and liquid level H=T. Four baffles with width of T/10 were mounted equally perpendicular to the vessel wall. Two six-bladed Rushton turbines with diameter of D=T/3 were used to mixing the fluid in the vessel. Height and width of the impeller blade were 20 mm and 25 mm, respectively. As listed in Table 1, three geometrical configurations were investigated by changing impeller spacing (C_2) and clearance from lower impeller to vessel bottom (C_1). In the literature, Rutherford *et al.* (1996) obtained parallel, merging and diverging flow patterns for these three configurations. Thus, for convenience, the geometry of the vessel in this work (Fig. 1) was named as "parallel", "merging" and "diverging" geometrical configuration, respectively. Four Netwtonian fluids were used in the simulation. Working media were glycerol solution with different concentration and the properties were listed in Table 2. In addition, in the following section, vessels with three dimensions (0.147 m, 0.294 m 0.588 m) of the parallel configuration were used to investigate scale-up characteristics. All parts in the vessels were enlarged with the same scale. Simulation methods for the vessel with different dimensions were the same as that of the vessel with diameter T=0.294 m.

2.2 Modeling and Grid Division

Considering the symmetry of geometry and the periodicity of fluid flow, only half of the vessel was used as solution domain. A multiple reference frame (MRF) technique was employed to solve the impeller rotation. While implementing the MRF technique, solution domain was divided into impeller region and other stationary region. Figure 2 shows the location of the two regions for different geometrical configurations. For all the configurations, radial location of the boundary between two regions was at r/R = 0.45. As for the axial boundary, the impeller region contained two parts for parallel and diverging configurations. The specific dimensions of the axial boundary for the two regions were listed in Table 3. Hybrid meshes were generated for the stirred vessels using software Gambit 2.4. The impeller region was divided with adaptable tetrahedral mesh, since the complicated structure of impellers. The other stationary region was divided with hexahedral mesh to reduce grids number and improve calculation accuracy. The important parts, such as surfaces of

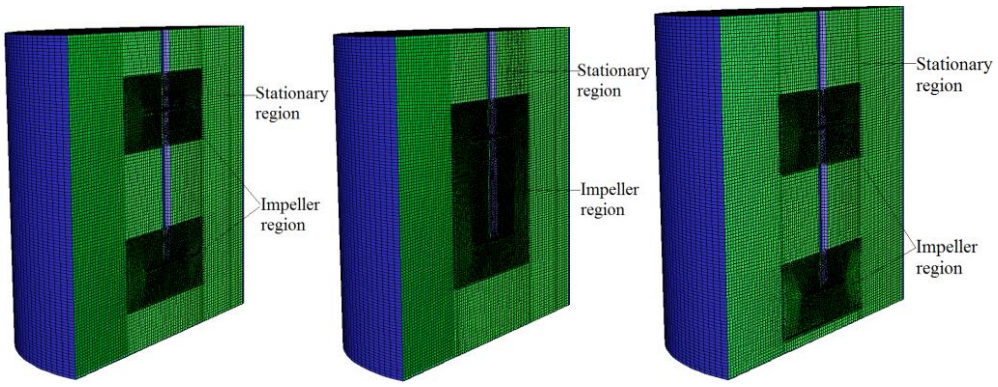

(a) Parallel (b) Merging (c) Diverging

Fig. 2. Mesh for the stirred vessel with different geometrical configurations.

impeller blades, interfaces of two regions were divided with refined meshes. Grid independence was tested by comparing the predicted total power number of different grid numbers. As listed in Table 4, the total power number with three grid numbers has bee studied for the parallel geometrical configuration. In this study, working medium is 94% glycerol solution for the laminar regime and pure water for the turbulent regime, respectively. It can be seen that total power number almost remains unchanged when grid number increases from 343672 to 748423, regardless of laminar or turbulent regime. Then, the grid number of 541260 is selected for the parallel geometrical configuration. Similar grid independence analysis method can also be found in Refs. (Achouri *et al.*, 2012; Wadnerkar *et al.*, 2012). Finally, the grid numbers for the fluid domain of the three geometrical configurations were 541260, 594233, 515362, respectively. Figure 2 shows grid division for the vessel with three geometrical configurations.

Table 3 Axial boundary of two regions for different geometrical configurations

Geometrical configuration	Axial boundary of two regions
Parallel	Part 1: 38 mm < z < 108 mm, Part 2: 185 mm < z < 255 mm
Merging	62 mm < z < 232 mm
Diverging	Part 1: 9 mm < z < 79 mm, Part 2: 156 mm < z < 226 mm

Table 4 Predicted total power number with different grid numbers for parallel geometrical configuration

Grid number	Reynolds number	Torque (N·m)	Power number
343672	50	0.01970	7.89
541260	50	0.01968	7.88
748423	50	0.01980	7.93
343672	2×10^4	0.02790	8.95
541260	2×10^4	0.02784	8.93
748423	2×10^4	0.02772	8.90

2.3 Governing Equations

2.3.1 Continuity and Momentum Equations

Flow fields in the stirred vessels were simulated by solving mass and momentum conservation equations as:

Mass conservation equation

$$\frac{\partial \rho}{\partial t}+\frac{\partial \rho u_i}{\partial x_i}=0 \tag{1}$$

where t is flow time and u_i is liquid component velocity of i direction.

Momentum conservation equation

$$\begin{aligned}&\frac{\partial(\rho u_i)}{\partial t}+\frac{\partial(\rho u_i u_j)}{\partial x_j}\\&=-\frac{\partial p}{\partial x_i}+\frac{\partial}{\partial x_j}\left[\mu\left(\frac{\partial u_i}{\partial x_j}+\frac{\partial u_j}{\partial x_i}-\frac{2}{3}\delta_{ij}\frac{\partial u_k}{\partial x_k}\right)\right]\\&+\frac{\partial}{\partial x_j}\left(-\rho\overline{u_i' u_j'}\right)\end{aligned} \tag{2}$$

where p and μ are static pressure and molecular viscosity, respectively. u_i' is fluctuating velocity components (i=1, 2, 3). $-\rho\overline{u_i' u_j'}$ represents Reynolds stress. In turbulent flow regime, Reynolds stress is modeled as:

$$-\rho\overline{u_i' u_j'}=\mu_t\left(\frac{\partial u_i}{\partial x_j}+\frac{\partial u_j}{\partial x_i}\right)-\frac{2}{3}\left(\rho\kappa+\mu_t\frac{\partial u_\kappa}{\partial x_\kappa}\right)\delta_{ij} \tag{3}$$

where κ is turbulence kinetic energy, and μ_t is turbulent viscosity, which are obtained by solving the standard κ-ε turbulent model when fluid flow field was in turbulent regime in this work.

2.3.2 Turbulence Model

Flow regime in a stirred vessel can be determined with Reynolds number as:

$$Re = \frac{D^2 N \rho}{\mu} \tag{4}$$

In this work, the flow field in laminar regime was studied with $Re \leq 100$ and that in turbulent regime with $Re \geq 2\times10^4$. In turbulent regime, the turbulent flow can be predicted using different turbulence models, such as Spalart-Allmaras (1992), κ-ε (Launder and Spalding, 1972), SST κ-ω (Lin *et al*., 2018) models and Reynolds stress model (Pope, 2000), etc. In these models, the standard κ-ε model has been widely used since it can provide reasonable accuracy in a wide range of turbulent flows. Thus, the standard κ-ε turbulence model was used to describe turbulent flow in the vessel. The standard κ-ε turbulence model includes two equations, i.e. kinetic energy κ and turbulent energy dissipation rate ε as:

$$\frac{\partial}{\partial t}(\rho\kappa) + \frac{\partial}{\partial x_i}(\rho\kappa u_i) = \frac{\partial}{\partial x_j}\left[\left(\mu + \frac{\mu_t}{\sigma_\kappa}\right)\frac{\partial \kappa}{\partial x_j}\right] + G_\kappa + G_b - \rho\varepsilon - Y_M \tag{5}$$

$$\frac{\partial}{\partial t}(\rho\varepsilon) + \frac{\partial}{\partial x_i}(\rho\varepsilon u_i) = \frac{\partial}{\partial x_j}\left[\left(\mu + \frac{\mu_t}{\sigma_\kappa}\right)\frac{\partial \varepsilon}{\partial x_j}\right] + C_{1\varepsilon}\frac{\varepsilon}{\kappa}(G_\kappa + C_{3\varepsilon}G_b) - C_{2\varepsilon}\rho\frac{\varepsilon^2}{\kappa} \tag{6}$$

where G_κ is the generation of turbulence kinetic energy due to the mean velocity gradients, and can be calculated as:

$$G_\kappa = -\rho\overline{u_i' u_j'}\frac{\partial u_j}{\partial x_i} \tag{7}$$

G_b represents the production of turbulence kinetic energy due to buoyancy and is not considered in this study. Y_M is the effect of the fluctuating dilatation in compressible turbulence on the overall dissipation rate, which is normally neglected for incompressible flows. By solving above equations, turbulence kinetic energy (κ) and its dissipation rate (ε) are obtained. Then, the turbulent viscosity μ_t in Eq. (3) is computed by:

$$\mu_t = \rho C_\mu \frac{\kappa^2}{\varepsilon} \tag{8}$$

The model constants for the standard κ-ε turbulent model are $C_{1\varepsilon}$ =1.44, $C_{2\varepsilon}$ =1.92, C_μ =0.09, σ_κ=1.0, σ_ε =1.3, respectively.

2.4 Computation Details

The commercial CFD package Fluent 6.3 was used to perform the numerical simulation. As mentioned previously, a multiple reference frame (MRF) approach was used to model impeller rotation. The impeller region was solved under rotational reference frame with speed equal to impeller speed N, and the other region was solved under stationary reference frame. The faces between two regions were defined as "interfaces", and the mass and momentum of two regions were exchanged through these interfaces. The solid walls, such as surfaces of tank internal wall, shaft and impeller were defined as nonslip boundary conditions and a standard wall function was used to treat the turbulent flow in near-wall regions. Moreover, a pair of periodic boundary condition was imposed to link fluid flow for the impeller region and stationary region, respectively. The coupling of pressure and velocity was obtained using a SIMPLE algorithm. Second order upwind scheme was employed for discretization of all terms of the governing equations.

2.5 Model Validation

The reliability and accuracy of simulation results in laminar and turbulent flow regimes are verified, respectively. Model validation in laminar regime was carried out in a vessel stirred by three Rushton turbine with diameter of T=0.24 m. The geometry of the vessel was consistent with the experimental vessel by Zalc *et al*. (2001). Firstly, flow field was simulated in the verifying stirred vessel. And then, the predicted velocity profiles were compared with experiment data in the literature (Zalc *et al.*, 2001). As shown in Fig. 3, the predicted axial and radial velocity profiles in laminar regime(Re=80) were in good agreement with experimental data in the literature (Zalc *et al.*, 2001). It should be pointed out that the simulation method for model validation is the same as that carried out in the dual-impeller vessels in this work. Therefore, the model validation can verify the simulation results in laminar flow regime in this work.

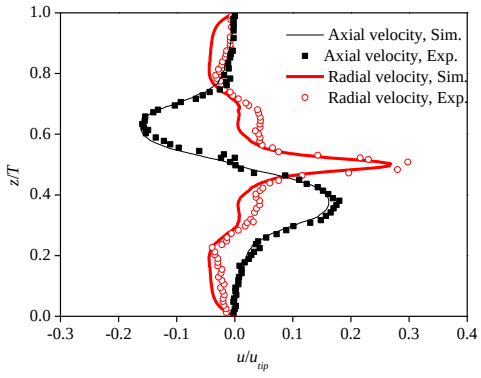

Fig. 3. Comparison of simulated velocity profiles with experimental data in the literature in laminar regime(r/R=0.5, Re=80).

As for the model validation in turbulent regime, the predicted velocity distributions in this work are compared with measurement results by Rutherford *et al.* (1996) using a laser-Doppler anemometer(LDA) technique. The vessel structure for model validation is consistent with that in this work with parallel configuration. The standard κ-ε model was used to describe the turbulent flow in the simulation of model validation. Figure 4 shows the predicted axial distributions of dimensionless radial velocity (u_r/u_{tip}) at two radial locations midway of two adjacent baffles and the

corresponding experimental data in the literature (Rusherford *et al.*, 1996; Micale *et al.*, 1999). The simulation results show good consistent with experiment data, which verify the reliability and accuracy of the simulation in turbulent regime.

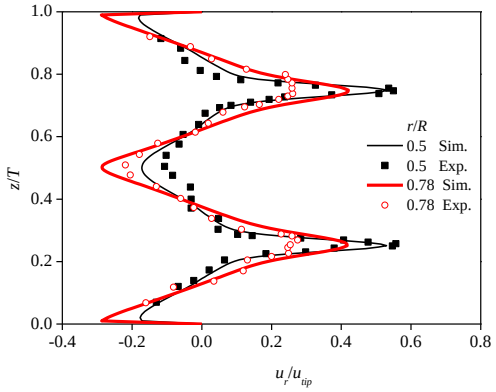

Fig. 4. Comparison of simulated radial velocity distributions with experimental data in the literature in turbulent regime (*N*=250 r/min, *Re*=4×10^4).

3. RESULTS AND DISCUSSION

3.1 Flow Field Characteristics in Laminar and Turbulent Regimes

Figure 5 shows fluid flows in the stirred vessel with different Reynolds numbers. To obtain different Reynolds numbers, the working medium is 94% glycerol solution for laminar flow regime ($Re \leq 100$) and that is water for turbulent flow regime ($Re \geq 2\times10^4$). It can be seen that the typical two-loop flow pattern forms for each Rushton turbine, which is the typical characteristics for a radial impeller. However, the flow pattern changes with Reynolds number in laminar regime. At very low Reynolds number (Re=25), the high liquid velocity is mainly concentrated in impeller region. The flow field in the stirred vessel is not fully developed. With increasing of Reynolds number, liquid velocity in most of regions increases, especially in near-wall regions. Figure 6 shows the axial distribution of dimensionless velocity (u/u_{tip}) at three radial locations. For the laminar regime, at the radial location close to blade tips (r/R=0.36), the dimensionless velocity almost keeps unchanged at the height of two impellers with increasing of Reynolds number, while that decreases at the other height of that radial location. For the radial location of r/R=0.5, the dimensionless velocity at impeller heights rises obviously for larger Reynolds numbers, while that in other heights decreases slowly. When the radial location close to near-wall regions (r/R=0.78), the dimensionless velocity for all heights rises with increasing of Reynolds number, especially that at impeller heights. The simulation results show that the dimensionless velocity at impeller heights in the stirred vessel gets the largest rise with increasing of Reynolds number or impeller speed in laminar regime. In addition, the absolute velocity is small in near-wall region ($r/R \geq 0.78$) for very low Reynolds number, and the impeller rotation has little effect on the velocity there. Nevertheless, the variation of flow pattern and dimensionless velocity in turbulent regime are different from that in laminar regime. As shown in Fig. 5(b) and Fig. 6(b), Reynolds number has little effects on flow pattern and dimensionless velocity distribution in turbulent regime.

3.2 Effect of Working Medium on Flow Field Characteristics for Laminar and Turbulent Regimes

Figure 7 shows the predicted flow patterns in the vessel with different working media. It can be seen that absolute velocity is different at the same Reynolds number due to the different physical properties of working media and impeller speeds. However, the flow pattern generated in the vessel is almost the same at the same Reynolds number, no matter it is in laminar or turbulent regime. Moreover, as shown in Fig. 8, the axial distribution of dimensionless velocity at the same Reynolds number is almost coincidence with different working media for laminar and turbulent regimes. Recently, Zhang *et al.* (2017) found that liquids with different viscosity but stirred at the same Reynolds number generated the same dimensionless velocity fields although in transitional flow regime.

In addition, the total impeller power numbers for different working media were predicted from the simulation results. In laminar regime (Re=50), the predicted total power number is 7.86, 7.88 and 7.89 for the glycerol solution with concentration of 75%, 94% and 100%, respectively. In turbulent regime (Re=2×10^4), the predicted total power number is 8.93 and 8.92 for water and 75% glycerol solution, respectively. Thus, from the simulation results, it can be concluded that flow pattern and power number in laminar and turbulent regimes for a given vessel depend mainly on the Reynolds number, and are hardly affected by working medium.

3.3 Scale-up Characteristics for the Stirred Vessel in Laminar and Turbulent Regimes

In order to investigate the effect of vessel scale-up on the flow pattern, the flow field characteristics in stirred vessels with different dimensions are numerically simulated. The working medium is 94% glycerol solution for laminar regime (Re=50) and that is water for turbulent regime (Re=2×10^4). For the vessels with diameter from 0.147 m to 0.588 m, all parts in the vessel were enlarged with the same scale. As shown in Fig. 9, although the absolute velocity changes with the dimension of the vessel, the flow pattern is almost unchanged at the same Reynolds number regardless of laminar or turbulent regimes. For further study, as shown in Fig. 10, the distributions of dimensionless velocity along dimensionless height are compared. No matter in laminar or turbulent regime, the distributions of dimensionless velocity in vessels are almost identical at the same Reynolds number, and are hardly affected by the dimensions of the

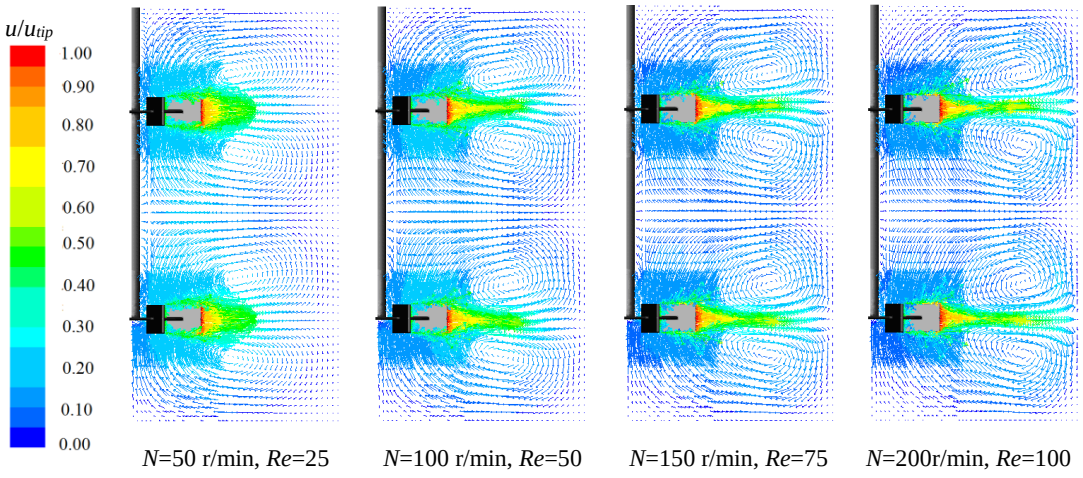

(a) Flow pattern in laminar regime

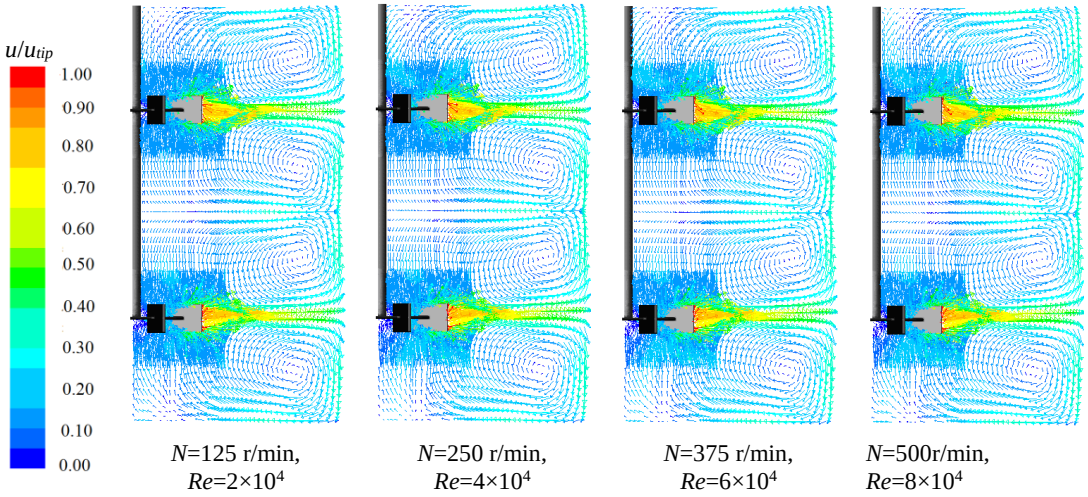

(b) Flow pattern in turbulent regime

Fig. 5. Flow patterns in the stirred vessel for laminar and turbulent regimes.

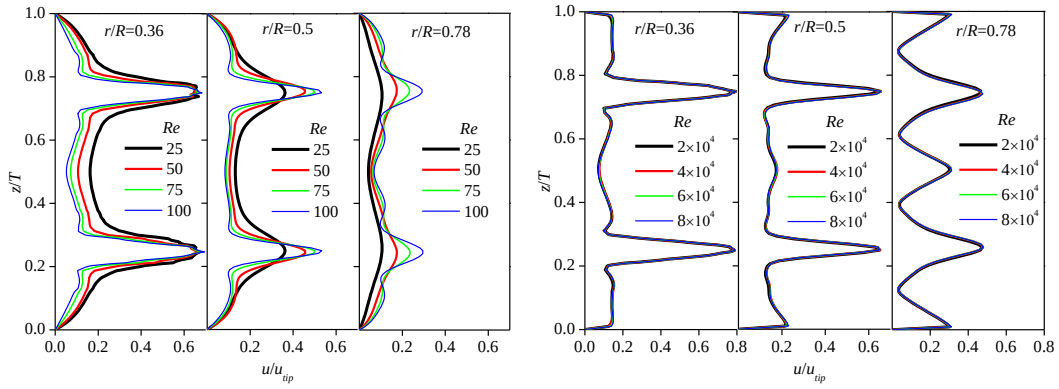

(a) For laminar flow regime (b) For turbulent flow regime

Fig. 6. Axial distributions of dimensionless velocity in vertical plane midway between baffles for laminar and turbulent regimes.

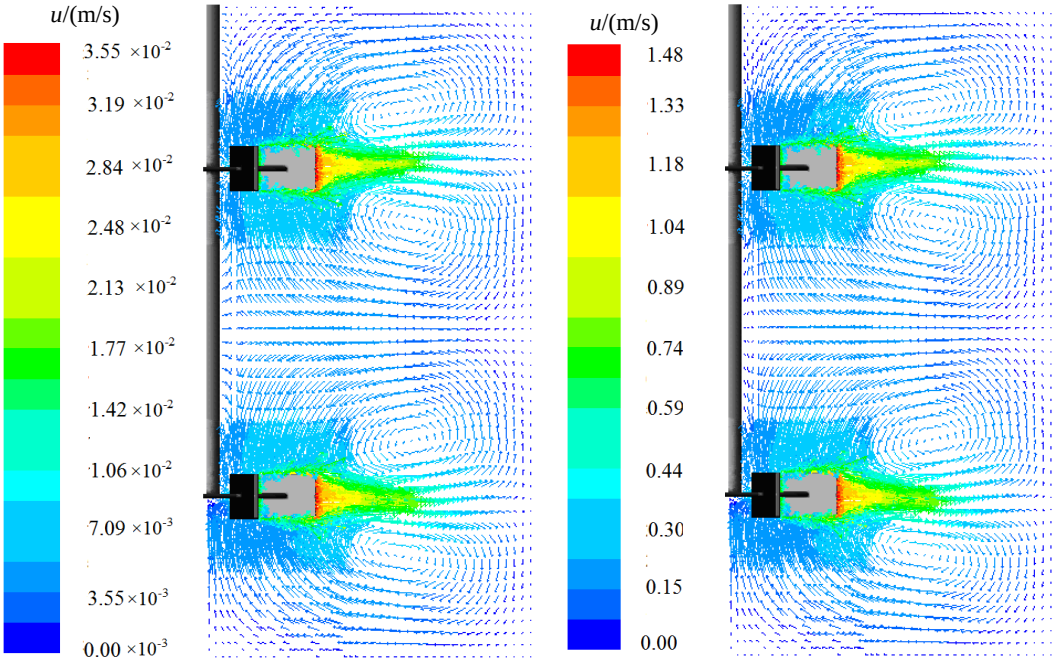

Glycerol concentration 75 %, *N*=6.9 r/min　　Glycerol concentration 100 %, *N*=288 r/min

(a) Reynolds number *Re*=50

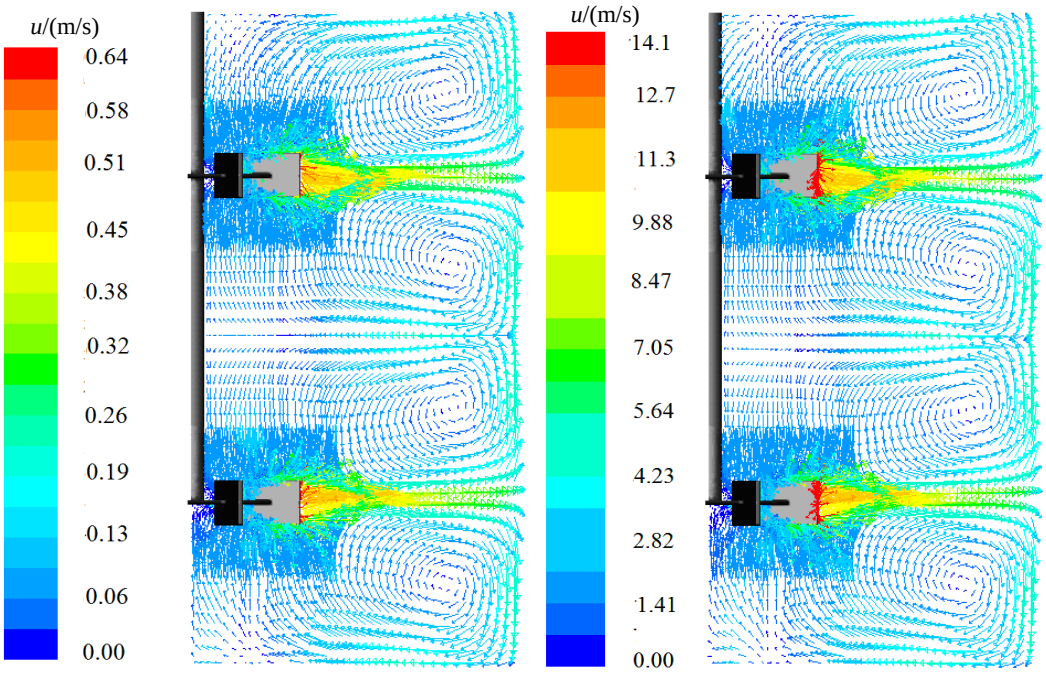

Glycerol concentration 0 %, *N*=125 r/min　　Glycerol concentration 75 %, *N*=2750 r/min

(b) Reynolds number *Re*=2×10^4

Fig. 7. Flow patterns in the stirred vessel with different working media in laminar and turbulent regimes.

vessel. Moreover, as listed in Table 5, the vessel size has little influence on the total impeller power number. The simulation results show that impeller power number is mainly the function of Reynolds number for the stirred vessel with a given geometrical configuration.

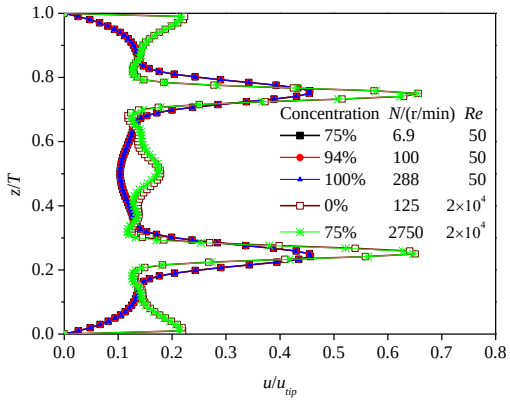

Fig. 8. Axial distributions of liquid velocity with different working media in laminar and turbulent regimes (*r*/*R*=0.5).

Table 5 Total impeller power number for vessel with different dimensions in laminar and turbulent regimes

T/mm	*N*/(r/min)	*Re*	*Np*
147	400	50	7.89
	500	2×10^4	8.92
294	100	50	7.88
	125	2×10^4	8.93
588	25	50	7.85
	31.3	2×10^4	8.91

3.4 Effect of Geometrical Configurations on Flow Patterns for Laminar and Turbulent Regimes

As the reviews previously, some scholars have found that parallel, merging and diverging flow patterns formed in turbulent regime in dual-Rushton stirred vessels. However, the variations of flow pattern in laminar regime are rarely studied. Figure 11 shows the predicted flow patterns in the vessel with different geometrical configurations in laminar and turbulent regimes. It can be seen that parallel, merging and diverging flow patterns form in the stirred vessel in turbulent regime (Re=4.0×10^4) by changing impeller spacing and off-bottom clearance of lower impeller. The simulation results are in good agreement with experimental observations (Rutherford *et al.*, 1996; Ranade *et al.*, 1997; Micale *et al.*, 1999; Liu *et al.*, 2008; Li *et al.*, 2007; Pan *et al.*, 2008). Moreover, as discussed in the previous section, flow patterns are no longer changed with Reynolds numbers in turbulent regime for a given configuration. Nevertheless, flow fields change with Reynolds number in laminar regime for a given configuration.

The change of flow pattern for parallel configuration has been discussed in the previous section and did not repeat here. As shown in Fig. 11(b), for the merging flow configuration, flow pattern is something similar to that formed by the combination of downward and upward pitched blade impellers. Moreover, the flow pattern varies with Reynolds numbers in laminar regime. When the Reynolds number is very low (Re≤25), the merging flow is not formed obviously even though the fluid discharge from the two impellers is inclined to each other. It is formed a large circular loop and a small circular loop for each impeller. With increasing of Reynolds number, the fluid discharge direction from blade tips is more inclined to each other, the two large circular loops are close to each other and the two small loops between two impellers reduce gradually to disappear. Then, the merging flow pattern is formed in the vessel. The merging flow pattern is very similar to that formed by a single Rushton turbine that mounted at the middle height of the vessel. In turbulent regime, the fluid flow is full developed, and the flow pattern is no longer change with Reynolds number. As for the diverging flow configuration, the flow pattern is different for the upper and lower impeller (Fig. 11(c)). The upper impeller generates the typical two-loop flow pattern with one circular loop above and the other below the impeller. For the lower impeller, the flow pattern is similar to that by a downward pitch blade impeller. When the Reynolds number is very low (Re=25), the inclination direction to the vessel bottom is very small, and there is a small loop below the lower impeller. With increasing of Reynolds number, the inclination angle increases and the loop below the impeller becomes smaller. In the turbulent regime, there are mainly three circular loops, with two formed by upper impeller and one by lower impeller in the stirred vessel. It is mainly because that the circular loop below the lower impeller can not form due to the limited space, when the lower impeller is very close to the vessel bottom. The flow field generated by upper impeller occupies about 2/3, while that by lower impeller only about 1/3 of the stirred vessel.

For quantitative analysis, Fig. 12 gives the axial distributions of dimensionless velocity between two adjacent baffles at location of r/R=0.6. For the parallel configuration, there are two main velocity peaks at the impeller heights. With increasing of Reynolds number, the dimensionless velocity increases mainly at the location of two impeller heights. Moreover, the dimensionless velocity in the surface and bottom regions increases obviously in turbulent regime. In particular, for the turbulent regime, a small velocity peak forms at the middle height where the flows generated by two impellers join together. For the merging configuration, there are two velocity peaks for very low Reynolds number (Re≤25), and the two peaks merged into one peak between the two impellers for high Reynolds numbers. Similar to the parallel configuration, dimensionless velocity increases obviously in the surface and bottom regions in turbulent regime. There are also two velocity peaks for the diverging configuration. With increasing of

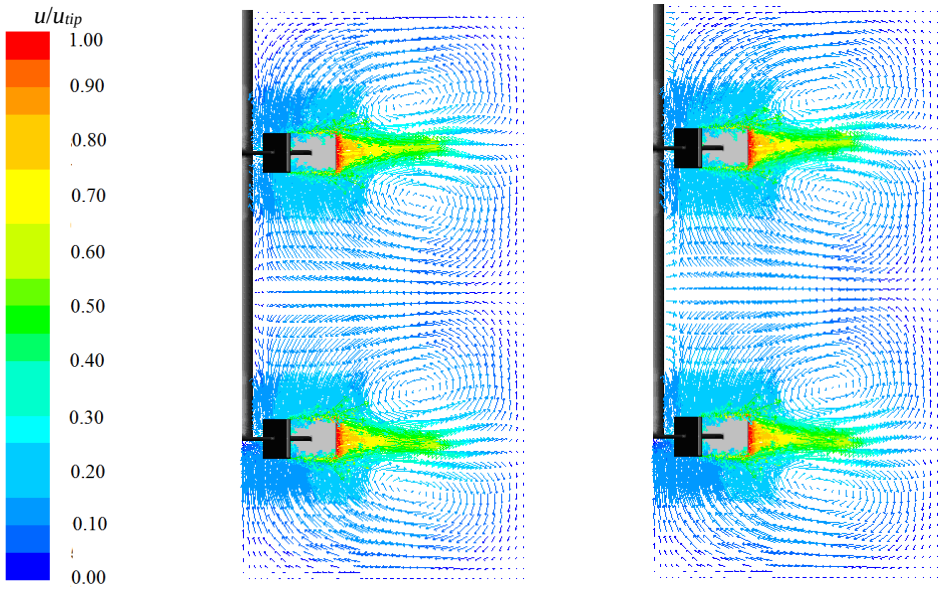

T=147 mm, *N*=400 r/min *T*=588 mm, *N*=25 r/min

(a) Reynolds number *Re*=50

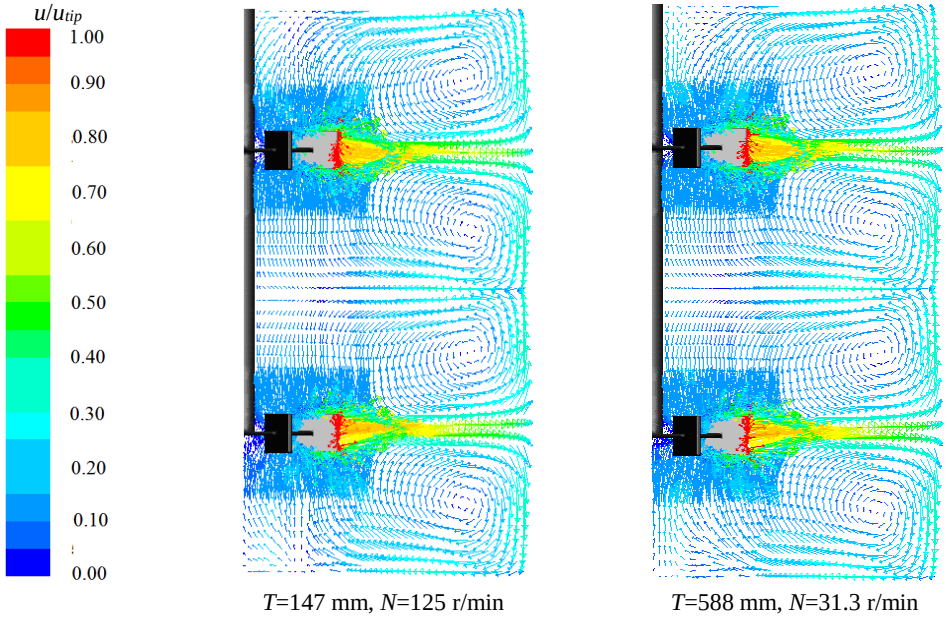

T=147 mm, *N*=125 r/min *T*=588 mm, *N*=31.3 r/min

(b) Reynolds number *Re*=2×10^4

Fig. 9. Flow pattern in the stirred vessels with different scale-ups in laminar and turbulent regimes.

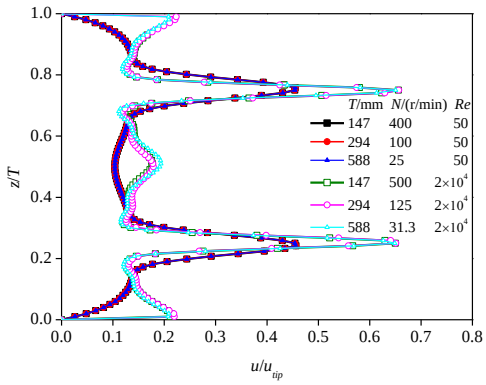

Fig. 10. Axial distributions of liquid velocity with different vessel scale-ups in laminar and turbulent flow regimes (*r*/*R*=0.5).

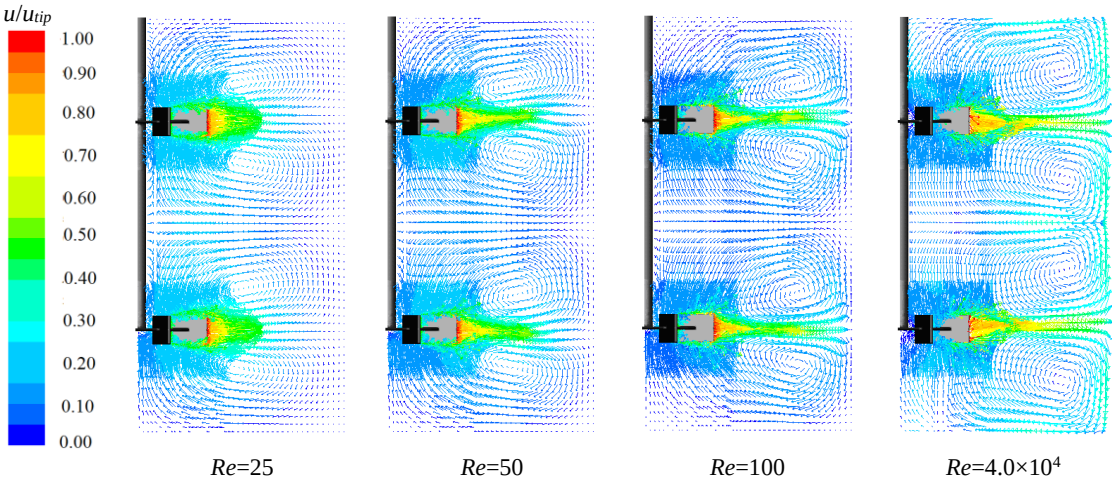

(a) Parallel configuration

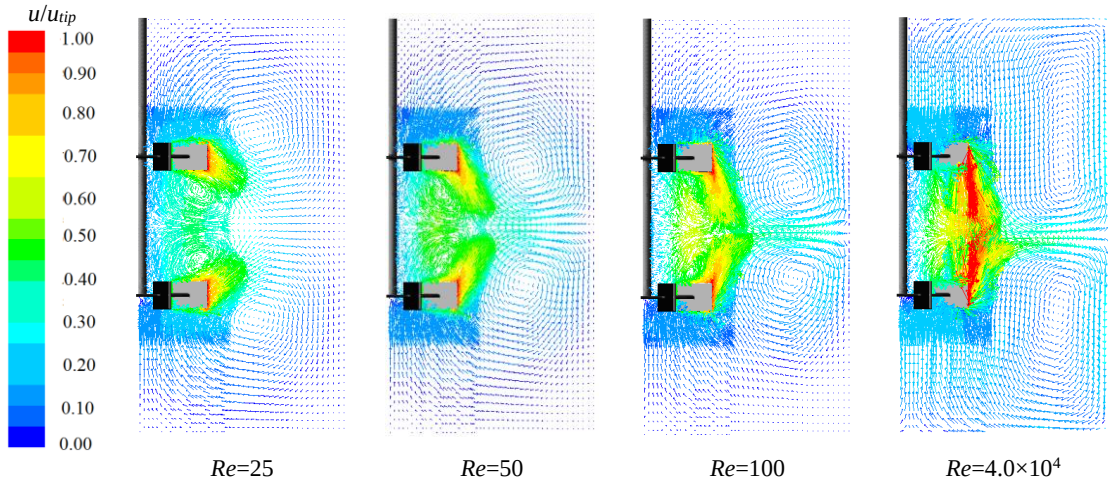

(b) Merging configuration

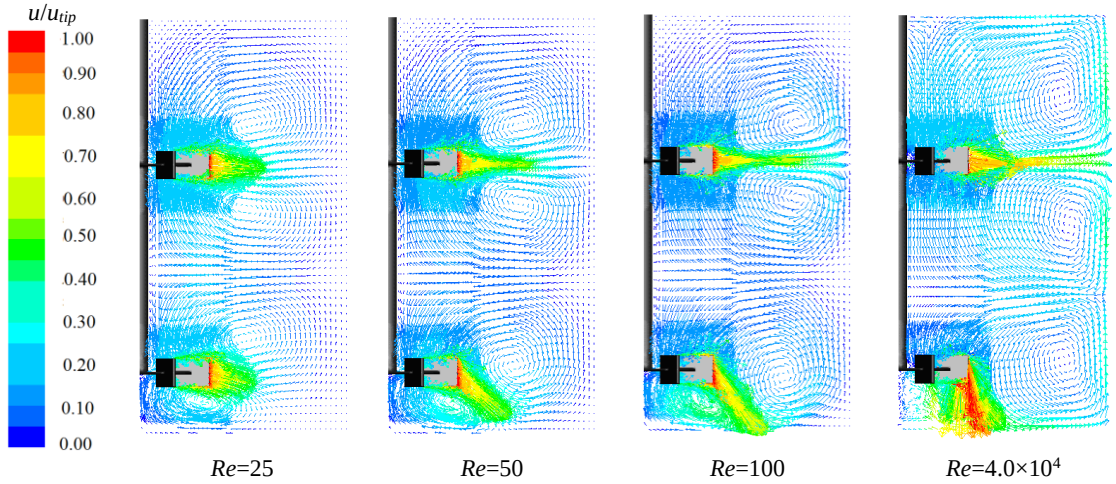

(c) Diverging configuration

Fig. 11. Flow patterns for laminar and turbulent regimes with different geometrical confirmations.

Reynolds number, the upper peak increases at the impeller height, while the lower peak moves gradually to vessel bottom. This is mainly due to the direction of fluid discharge for the lower impeller increases with increasing of Reynolds number (See Fig. 11).

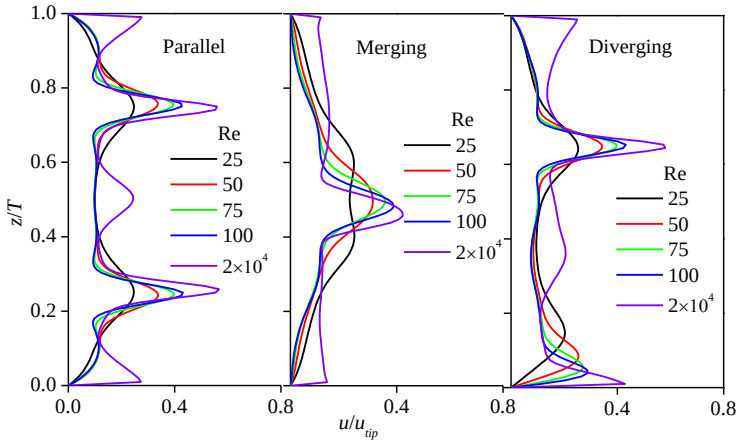

Fig. 12. Axial distributions of relative velocity in vertical plane midway between baffles for different geometrical configurations (*r*/*R*=0.6).

3.5 Power Number in the Stirred Vessel for Laminar and Turbulent Regimes

Power consumption is an important parameter for evaluating the performance of a stirred vessel. Power consumption and power number can be calculated from the simulation results as:

$$P=2\pi T_0 N \tag{9}$$

$$Np=\frac{P}{\rho N^3 D^5} \tag{10}$$

where T_0 is impeller torque in the rotational direction, which contains pressure torque and viscous torque and can be determined directly from simulation results.

As shown in Fig. 13, the geometrical configuration has significant effect on power number in laminar and turbulent regimes in the stirred vessel. Both in laminar and turbulent regimes, the total power number abided by the following order: Parallel>Diverging>Merging. Nevertheless, the variations of power number with Reynolds number are different for the two flow regimes. As shown in Fig. 13(a), total power number falls with increasing of Reynolds number in laminar regime. The power number of merging configuration gets the biggest drop, followed by diverging configuration, and lowest drop for the parallel configuration. Different from the laminar regime, total power number rises slightly in turbulent flow regime (Fig. 13(b)). When the Reynolds number increases from 2×10^4 to 8×10^4, total power number rises by 1.9%, 2.29% and 0.25% for the parallel, merging and diverging configuration, respectively. In general, Reynolds number, or impeller speed has little effect on power number in turbulent regime. In the literature (Rushton *et al.*, 1950; Wang and Feng, 2000; Deglon and Meyer, 2006), scholars such as Rushton *et al.* (1950) and Deglon *et al.* (2006) also found power number decreases in laminar regime and rises slightly in turbulent regime when the vessel was stirred by a Rushton turbine. On an average, the predicted total power number is 9.0, 7.15 and 8.15 for the parallel, merging and diverging flow in turbulent regime in this work, respectively. Rutherford *et al.* (1996) measured the total power number was 10, 8.4 and 9.5 at impeller speed of 250 r/min for the corresponding flow patterns, respectively. The simulation results are in good agreement with the experimental data (Rutherford *et al.*, 1996).

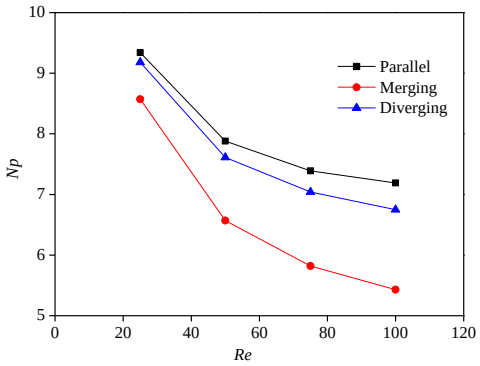

(a) Total impeller power number in laminar regime

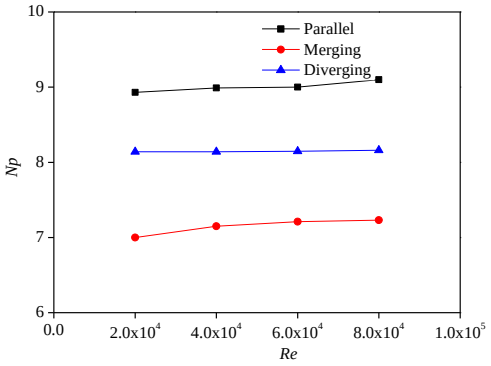

(b) Total impeller power number in turbulent regime

Fig. 13. Total impeller power number for different configurations in laminar and turbulent flow regimes.

Furthermore, power number for each impeller in laminar and turbulent regimes was investigated as

shown in Fig. 14. Generally, for each configuration, the variation of single-impeller power number with Reynolds number is similar to that of total power number. The power number of upper and lower impeller is very close for parallel and merging configurations, while the power number of upper impeller is much higher than that of lower impeller for diverging configuration. The power number of upper impeller for diverging configuration is the highest in both flow regimes. The main reason may be that the space of upper impeller region is very large for the diverging configuration. The fluid in the lower impeller region of the diverging configuration can not flow well due to blocking effect of the vessel bottom. As a result, the power number of lower impeller for the diverging configuration is much smaller than that of upper impeller, especially, that is the lowest in the turbulent regime.

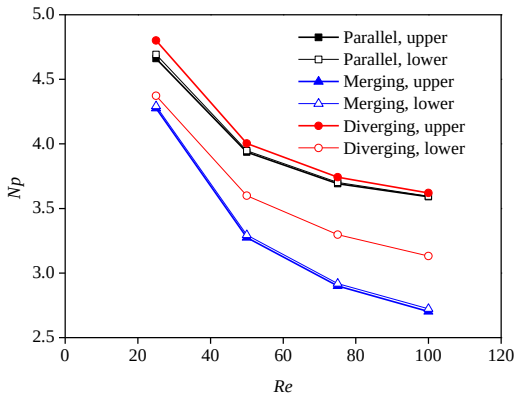

(a) Impeller power number in laminar regime

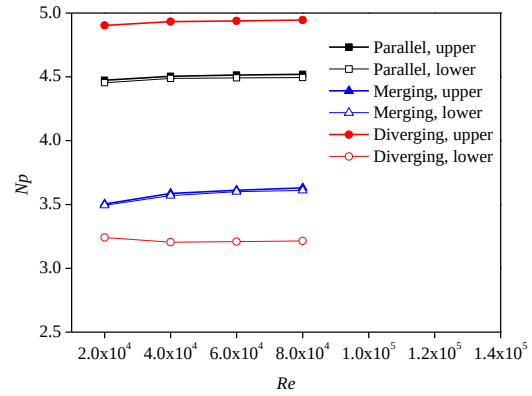

(b) Impeller power number in turbulent regime

Fig. 14. Power number for each impeller in laminar and turbulent flow regimes.

4. CONCLUSION

A comparative CFD study on laminar and turbulent flow field characteristics in a vessel stirred by dual Rushton turbines has been carried out in this work. The main conclusions were drawn as follows.

(1) In laminar regime, flow field and dimensionless velocity in the stirred vessel vary with Reynolds number, while those keep unchanged with different work media at the same Reynolds number. For parallel configuration, the dimensionless velocity at impeller heights gets the largest rise in laminar regime with increasing of Reynolds number. In turbulent regime, flow pattern and dimensionless velocity distribution are little affected by both Reynolds number and working medium.

(2) When the stirred vessel was enlarged with all parts the same scale, flow pattern and dimensionless velocity distribution are coincident in the vessels with different sizes as long as the Reynolds number is the same, regardless in laminar or turbulent flow regime.

(3) By changing impeller spacing and clearance of lower impeller from the vessel bottom, parallel, merging and diverging flow patterns were obtained in turbulent regime. In laminar regime, the flow patterns are not fully developed and change with Reynolds numbers for the three geometrical configurations.

(4) For the stirred vessel with a given geometrical configuration, the power number was mainly the function of Reynolds number, and little affected by working medium and enlargement scale. The total power number has the order of parallel>diverging>merging for the three configurations at the same Reynolds number. With the increase of Reynolds number, the drop of total power number is the largest for merging configuration, followed by diverging configuration, and lowest drop for parallel configuration in laminar regime, while gets slight rise of total power number for the three configurations in turbulent regime.

ACKNOWLEDGEMENTS

The authors would like to acknowledge the support by National Green Manufacturing System Integration Project (2016), Ministry of Industry and Information Technology of China. Key Scientific Research Project of Sichuan Provincial Education Department (15ZA0107).

REFERENCES

Abradi, V., G. Rovero, S. Sicardi, G. Baldi and R. Conti (1988). Sparged vessels agitated by multiple impellers. *The 6th European Conference on Mixing*, 329-336.

Achouri, R., I. Mokni, H. Mhiri and P. Bournot (2012). A 3D CFD simulation of a self inducing pitched blade turbine downflow. *Energy conversion and management* 64(12), 633-641.

Albert, D., III. Harvey and K. C. Lee (1995). Steady-state modeling and experimental measurement of a baffled impeller stirred tank. *AIChE J* 41(10), 2177-2186.

Ascanio, G., M. Brito-Bazán, E. Brito-De La Fuente P. J. Carreau and P. A. Tanguy (2002). Unconventional configuration studies to improve mixing times in stirred tanks. *The Canadian Journal of Chemical Engineering* 80(4), 558-565.

Bakker, A., K. J. Myers, R. W. Ward and K. C. Lee (1996). The laminar and turbulent flow pattern of a pitched balde turbine. *Chemical Engineering Research and Design* 74(4), 485-491.

Cherry, R. S. and E. T. Papoutsakis (1988). Physical mechanisms of cell damage in microcarrier Cell Culture Bioreactors. *Biotechnology and Bioengineering* 32(8), 1001-1014.

Croughan, M. S., J. F. Hamel and D. I. C. Wang (2000). Hydrodynamic effects on animal cells grown in microcarrier cultures. *Biotechnology and Bioengineering* 67(6), 841-852.

Deglon, D. A. and C. J. Meyer (2006). CFD modeling of stirred tanks: Numerical considerations. *Minerals Engineering* 19(10), 1059-1068.

Fan L., W. J. Wang, C. Yang and Z. S. Mao (2004). Numerical simulation of laminar flow field in a stirred tank. *Chinese Journal of Chemical Engineering* 12(3), 324-329.

Foucault, S. G. Ascanio and P. A. Tanguy (2006). Mixing times in coaxial mixers with Newtonian and non-Newtonian fluids. *Industrial & Engineering Chemistry Research* 45, 352-359.

Gogate, P. R., A. A. C. M. Beenackers and A. B. Pandit (2000). Multiple-impeller systems with a special emphasis on bioreactors: a critical review. *Biochemical Engineering Journal* 6(2), 109-144.

Hudcova V., V. Machon and A. W. Nienow (1989). Gas-liquid dispersion with dual Rushton impellers. *Biotechnology and Bioengineering* 34(5), 617-628.

Kasat, G. R. and A. B. Pandit (2004). Mixing time studies in multiple impeller agitated reactors. *The Canadian Journal of Chemical Engineering* 82(5), 892-904.

Lamberto D. J., F. J. Muzzio and P. D. Swanson (1996). Using time-dependent RPM to enhance mixing in stirred vessels. *Chemical Engineering Science* 51(5), 733-741.

Lamberto, D. J., M. M. Alvarez and F. J. Muzzio (1999). Experimental and computational investigational investigation of the laminar flow structure in a stirred tank. *Chemical Engineering Science* 54(7), 919-942.

Launder, B. E. and D. B. Spalding (1972). *Lectures in mathematical models of turbulence*. Academic Press London, England.

Li, Z. P., Z. M. Gao, J. M. Smith and R. B. Thorpe (2007). Large eddy simulation of flow fields in vessels stirred by dual Rushton impeller agitators. *Journal of chemical engineering of Japan* 40(8), 684-691.

Liang, Y. N., D. R. Gao and L. Bai (2015). Numerical simulation of the laminar flow field and mixing time in stirred tank with double layer impeller. *Chinese Journal Mechanical Engineering* 51(6), 185-195.

Lin, A., Y. Sun, H. Zhang, X. Lin, L. Yang and Q. Zheng (2018). Fluctuating characteristics of air-mist mixture flow with conjugate wall-film motion in a compressor of gas turbine. *Applied Thermal Engineering* 142, 779-792.

Liu, X. H., Y. Y. Bao, Z. P. Li, Z. M. Gao and J. M. Smith (2008). Particle image velocimetry study of turbulence characteristics in a vessel agitated by a dual Rushton impeller. *Chinese Journal Chemical Engineering* 16(5), 700-708.

Mahmoudi, S. M. and M. Yianneskis (1992). The variation of flow pattern and mixing time with impeller spacing in stirred vessels with two Rushton impellers. *Fluid Mechanics of Mixing Springer*, Dordrecht 11-18.

Mao, D. M. (1998). Study on mixing and flow in vessels stirred by multi-deck impellers. *Doctoral dissertation. Zhejiang, University*, Hangzhou, China (In Chinese).

Miao, Y., J. Z. Pan, G. R. Niu, J. Min and Z. M. Gao (2006). Mixing in stirred tanks with multiple impellers. *Journal of East China University of Science and Technology* 32(3), 357-360.

Micale, G., A. Brucato, F. Grisafi and M. Ciofalo (1999). Prediction of flow fields in a dual-impeller stirred vessel. *AIChE J* 45(3), 445-464.

Millward, H. R. and B. J. Bellhouse (1994). Mammalian cell damage in novel membrane bioreactor. *Biotechnology and Bioengineering* 43(9), 899-906.

Pan, C., J. Min, X. Liu and Z. M. Zao (2008). Investigation of fluid flow in a dual Rushton impeller stirred tank using particle image velocimetry. *Chinese Journal of Chemical Engineering* 16(5), 693-699.

Pope S. B. (2000). *Turbulent Flows*, Cambridge University Press.

Puthli, M. S., V. K. Rathod and A. B. Pandit (2005). Gas-liquid mass transfer studies with triple impeller system on a laboratory scale bioreactor. *Biochemical Engineering Journal* 23(1), 25-30.

Ranade, V. V. and V. R. Deshpande (1997). Computational flow modeling of dual Rushton impeller stirred vessels. *47th Canadian Chemical Engineering Conference*.

Rice, M., J. Hall, G. Papadakis and M. Yianneskis (2006). Investigation of laminar flow in a

stirred vessel at low Reynolds numbers. *Chemical Engineering Science* 61(9), 2762-2770.

Rushton, J. H., E. W. Costich and H. J. Everett (1950). Power characteristics of mixing impellers-Part II. *Chemical Engineering Progress* 46(9), 467-476.

Rutherford, K., K. C. Lee, S. M. Mahmoudi and Yianneski (1996).Hydrodynamic characteristics of dual Rusthton impeller stirred vessels. *AIChE J* 42(2), 332-346.

Spalart, P. R. and S. R. Allmaras (1992). A one-equation turbulence model for Aerodynamic flows. *AIAA Paper* 92-439.

Wadnerkar, D., R. P. Utikar, M. O. Tade and V. K. Pareek (2012). CFD simulation of solid–liquid stirred tanks. *Advanced Powder Technology* 23, 445-453.

Wang, K. and L. F. Feng (2000). *Mixing equipment design*. Beijing: China Machine Press (In Chinese).

Weng Z. X. (1983). The effect of the distance between multiple impellers in the turbulent tank. *Chemical Engineering* 6, 1-6.

Woziwodzki, S., L. Broniarz-Press and M. Ochowiak (2010). Effect of eccentricity on transitional mixing in vessel equipped with turbine impellers. *Chemical Engineering Research and Design* 88(12), 1607-1614.

Zalc, J. M., E. S. Szalai, M. M. Alvarez and F. J. Muzzio (2002). Using CFD to understand chaotic mixing in laminar stirred tanks. *AIChE J* 48(10), 2124-2134.

Zalc, J. M., M. M. Alvarez and F. J. Muzzil (2001). Extensive validation of computed laminar flow in a stirred tank with three Rusthton turbines. *AIChE J* 47(10), 2144-2154.

Zhang Y. L. Z. M. Gao and Z. P. Li (2017). Transitional flow in a Rushton turbine stirred tank. *AIChE J* 63, 3610-3623.